ARMA 19-103

Propagation of a plane-strain hydraulic fracture accounting for the presence of a cohesive zone and a fluid lag

Liu, D.
EPFL, Lausanne, Switzerland
Lecampion, B.
EPFL, Lausanne, Switzerland

ABSTRACT: We revisit the problem of the propagation of a plane-strain fluid-driven fracture in a quasi-brittle impermeable medium accounting for the presence of a fluid lag. The fracture process zone is simulated using a linear-softening cohesive model while lubrication flow accounts for the possible occurence of a fluid lag. The solution is obtained numerically via a fully implicit scheme based on a boundary element method for the fracture deformation and finite difference for fluid flow. The fluid lag is first automatically captured using the Elrod-Adams lubrication cavitation model during the initiation and early stage of fracture growth. We then switch to an algorithm tracking the fluid front for computational efficiency. Using dimensional analysis, we show that the propagation is governed by a dimensionless toughness and a time scale characterizing the diappearance of the fluid lag (both similar to the linear elastic fracture mechanics case) and a ratio between the in-situ minimum confining stress and the material tensile strength. The cohesive forces reinforce the suction effect associated with a fluid lag, and leads to the further localization of the fluid pressure drop near the tip. This ultimately results in a slight increase of fracture opening and net pressure.

1. INTRODUCTION

Some discrepancies between predictions based on linear elastic fracture mechanics (LEFM) and observations from laboratory and field experiments - notably larger net pressure and shorter fracture length - have been reported by a number of authors (Shlyapobersky, 1985; Shlyapobersky *et al.*, 1988; Thallak *et al.*, 1993). These observations have been often associated with a process zone around the fracture tip where non-elastic processes such as large plastic deformations or micro-cracking are no longer negligible (Papanastasiou, 1997). A number of works have accounted for the presence of cohesive forces to study the effect of near-tip solid non-linearities on hydraulic fracture growth (Chen *et al.*, 2009; Chen, 2012; Lecampion, 2012; Yao *et al.*, 2015) demonstrating a similar fracture evolution to that of a linear elastic fracture. The importance of the influence of the level of confining stress and its interplay with the presence of a fluid lag have been recognized early by Rubin, 1993, but its impact on propagation has not been systematically investigated.

Cohesive zone models have been widely used in numerical simulations to account for the non-linear behavior of quasi-brittle materials at fracture. Such type of model requires a sufficient number of elements in the cohesive zone to ensure the accuracy of the numerical solution. Moës and Belytschko, 2002 suggest in the context of the extended finite element method to have at least two elements inside the cohesive zone. It is here important to note that at minima the mesh scale needs to resolve the tensile zone ahead of the fracture. This imposes a stronger mesh requirement as the in-situ compressive stress increases – a fact that has been seldom discussed in the context of hydraulic fracture propagation with cohesive zone models (Sarris and Papanastasiou, 2011; Carrier and Granet, 2012; Salimzadeh and Khalili, 2015; Wang, 2015; Wang *et al.*, 2016; Li *et al.*, 2017).

The existence of suction in the near tip region of a hydraulic fracture and the evolution of the fluid lag zone during hydraulic fracture growth is now well understood in the context of linear elastic fracture mechanics (Garagash and Detournay, 2000; Garagash, 2006; Lecampion and Detournay, 2007). Numerically, different algorithms have been proposed. Lecampion and Detournay, 2007 and Bunger, 2005 adopt a fully implicit moving mesh method and track the moving fronts of both the fracture tip and the fluid. A

fixed-grid algorithm is put forward by Zhang *et al.*, 2005 and Gordeliy and Detournay, 2011 who utilize a filling fraction factor / level set approach to model the evolution of the fluid front and the disappearance of the fluid lag with time. These different approaches require a known initial condition (where the fluid lag is maximum) - i.e. Garagash, 2006 for the plane-strain case. However, when investigating hydraulic fracture initiation and propagation using a cohesive zone approach, the quasi-brittle nature of the fracture process and its coupling with lubrication flow results in a different response for which no initial solution is available. The modeling of such phenomena therefore requires an approach modeling the spontaneous occurrence of the fluid lag. Recently, Shen, 2014 and Mollaali and Shen, 2018 have proposed two different approaches to automatically account for a fluid lag using respectively a variational inequality formulation and an algorithm borrowed from thin film lubrication cavitation. We have implemented both approaches and found that the Elrod-Adams method proposed in Mollaali and Shen, 2018 captures the fluid front position in the most accurate manner. These lubrication with cavitation algorithms are unfortunately computationally costly, and as such not well suited at large time when the extent of the fluid lag slowly decreases after the initial transient associated with fracture initiation.

In this paper, we develop an algorithm accounting for the presence of an evolving cohesive zone and a fluid lag. We first start our scheme using the Elrod-Adams method to model the early-time fracture growth and the spontaneous appearance of the fluid lag. As soon as the fluid lag has fully developed and the fluid front is starting to catch up the fracture tip, we switch to an algorithm based on the tracking of the fluid front (similar to the one described by Gordeliy and Detournay, 2011).

2. PROBLEM DESCRIPTION

We investigate the case of a plane-strain fracture driven by an incompressible Newtonian fluid under a constant injection rate in an infinite quasi-brittle impermeable medium. We denote w as the fracture width, p_f, the fluid pressure, σ_o as the far-field in-situ confining stress acting normal to the fracture plane and σ_{yy} as the stress component in the y direction ahead of the fracture tip as illustrated in Fig. 1.

Fluid cavitation may occur due to suction effects associated with the coupling between elastic deformation and fluid flow in the fracture resulting in a lag between the fluid front and fracture tip. Our objective is to investigate hydraulic fracture propagation accounting for the existence of both the cohesive zone and fluid lag.

The solution of the problem is given by the net fluid pressure $p(x,t) = p_f(x,t) - \sigma_o$, the fracture opening $w(x,t)$, the half fracture length $\ell(t)$, the cohesive zone length $\ell_{coh}(t)$

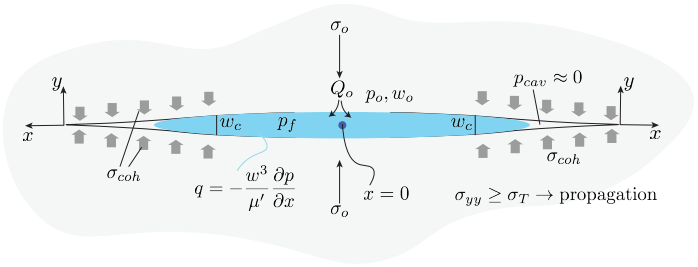

Fig. 1: Problem description

and the fluid front $\ell_f(t)$ as a function of the position x along the fracture and time t. We denote the injection rate as Q_o, while we use the following parameters for clarity

$$K' = \sqrt{\frac{32}{\pi}} K_{Ic}, \quad E' = \frac{E}{1-\nu^2}, \quad \mu' = 12\mu \tag{1}$$

where E is the solid elastic modulus, K_{Ic} fracture effective toughness for quasi-brittle solid, ν Poisson's ratio and μ the fluid viscosity.

We simulate the quasi-brittle behavior of the material at fracture via a linear-softening cohesive zone model. Cohesive tractions act on the fracture surface and decay linearly as function of aperture from the peak tensile strength to zero for fracture width larger than a critical opening

$$\sigma_{coh}(w) = \begin{cases} \sigma_T(1 - w_c) & 0 \leq w < w_c \\ 0 & w > w_c \end{cases} \tag{2}$$

where σ_T is the maximum cohesive traction and w_c the critical opening beyond which cohesive tractions vanish. The critical fracture energy of the material for such a linear softening law is therefore

$$G_c = \frac{1}{2}\sigma_T w_c = \frac{K_{Ic}^2}{E'} \tag{3}$$

which, using Irwin's relation, can be related to the fracture toughness K_{Ic} of the material upon the assumption of linear elastic fracture mechanics.

3. GOVERNING EQUATIONS

Elasticity For a pure Mode I plane-strain fracture propagating perpendicular to the minimum principal in-situ compressive stress, the elasticity reduces to a boundary integral equation relating the net pressure p to the fracture opening w which can be written accounting for the presence of cohesive forces (Hills *et al.*, 2013)

$$\frac{E'}{4\pi}\int_0^{\ell}\left(\frac{1}{x-x'} - \frac{1}{x'+x}\right)\frac{\partial w}{\partial x'}\mathrm{d}x' = p_f(x) - \sigma_o - \sigma_{coh}(w(x)) \tag{4}$$

where σ_o the in-situ compressive stress normal to the fracture plane is uniform.

Lubrication Under the assumption of zero leak-off, as the fluid compressibility is much smaller than the fracture elastic compliance, the width-averaged mass conservation reduces to the following volume conservation:

$$\frac{\partial w}{\partial t} + \frac{\partial q}{\partial x} = 0, \quad 0 < x < \ell_f \tag{5}$$

where the local fluid flux q is related to the local pressure gradient under the lubrication approximation

$$q = -\frac{w^3}{\mu'}\frac{\partial p_f}{\partial x}, \quad 0 < x < \ell_f \tag{6}$$

The viscous fluid flow in the fracture is therefore governed by

$$\frac{\partial w}{\partial t} = \frac{\partial}{\partial x}\left(\frac{w^3}{\mu'}\frac{\partial p_f}{\partial x}\right), \quad 0 < x < \ell_f \tag{7}$$

Boundary condition At the fracture center $x = 0$, injection of the fluid is idealized as a line source with a constant injection rate Q_o. The fracture front $x = \ell$ is constrained by zero fracture opening.

$$\lim_{x\to 0} q = Q_o, \quad w(\ell, t) = 0 \tag{8}$$

while in the fluid lag and at the fluid front boundary $\ell_f(t)$, we have the following:

$$p_f(x) = 0, \quad \ell_f \le x < \ell, \quad \dot{\ell}_f = -\frac{w^2}{\mu'}\left.\frac{\partial p_f}{\partial x}\right|_{x=\ell_f} \tag{9}$$

Global continuity equation By integrating the lubrication equation considering the inlet condition, one gets the global fluid balance,

$$2\int_0^{\ell_f} w \mathrm{d}x = Q_o t \tag{10}$$

Propagation criteria For a quasi-brittle medium, the onset of de-cohesion is controlled by the stress component perpendicular to the fracture plane σ_{yy},

$$\sigma_{yy} \ge \sigma_T \tag{11}$$

In linear elastic materials, a propagating fracture, as a result of LEFM, can be expressed as a limiting asymptote of the fracture opening at the tip.

$$w \sim \frac{K'}{E'}(\ell - x)^{1/2}, \quad 1 - x/\ell \ll 1 \tag{12}$$

Table 1: Viscosity scaling (M-scaling) and toughness scaling (K-scaling, an equivalent scaling, see Eq. (3), where the effective toughness dominates the hydraulic fracture propagation in quasi-brittle medium)

	M	K
ϵ	$\epsilon_m = \left(\frac{\mu'}{E't}\right)^{1/3}$	$\epsilon_m \mathcal{K}_m^{4/3}$
L	$L_m = \left(\frac{E'Q_o^3 t^4}{\mu'}\right)^{1/6}$	$L_m \mathcal{K}_m^{-2/3}$
$\mathcal{G}_k$	$\mathcal{K}_m = \frac{K'}{E'}\left(\frac{E'}{\mu' Q_o}\right)^{1/4}$	1
$\mathcal{G}_m$	1	$\mathcal{K}_m^{-4}$

4. DIMENSIONAL ANALYSIS

We scale the different variables focusing on a scaling emphasizing fracture toughness and viscosity following Garagash, 2006. We scale $w(x,t)$, $p_f(x,t)$, and $\ell(t)$ as follows:

$$w = \epsilon L \Omega, \quad p_f - \sigma_o = \epsilon E' \Pi, \quad \ell = L\gamma \tag{13}$$

We also define the normalized position along the fracture $\xi = x/\ell$, the dimensionless cohesive length $\xi_{coh} = \ell_{coh}/\ell$ and fluid front location $\xi_f = \ell_f/\ell$. We denote the viscosity scaling and toughness scaling respectively by subscript m and k. The expressions for the length scale L and the small number ϵ are shown in Table 1 where $\mathcal{G}_m$ and $\mathcal{G}_k$ are dimensionless groups. These scalings are similar to the one obtained assuming linear elastic fracture mechanics by defining a corresponding fracture toughness using Eq. (3), i.e. $K_{Ic} = \sqrt{G_c E'} = \sqrt{\sigma_T w_c E'/2}$. In the case of a cohesive zone, the solution is function of an additional dimensionless parameter relating the ratio of in-situ confinement to tensile strength σ_o/σ_T .

Note that we can also define a length scale w_μ characterizing the opening at the fluid front like in Garagash, 2015, and its ratio with critical opening w_c which characterizes the boundary of the cohesive zone

$$w_\mu = \left(\frac{\mu' E' Q_o}{\sigma_o^2}\right)^{1/2}, \quad \frac{w_c}{w_\mu} = \frac{\pi}{16}\frac{\sigma_o}{\sigma_T}\mathcal{K}_m^2 \tag{14}$$

The penetration of the cohesive zone by the fluid is linked to w_c/w_μ and thus ultimately to σ_o/σ_T and the dimensionless fracture toughness $\mathcal{K}_m$ (see Table 1). This expression agrees with the intuition that a larger confining stress tends to push the fluid toward the fracture tip and results in a larger penetration degree of the cohesive zone.

We will formulate the problem in a time-domain viscosity scaling similar to Lecampion and Detournay, 2007. The solution $(\gamma_m, \xi_f, \xi_{coh}, \Omega_m, \Pi_m)$ therefore depends on the normalized position ξ, the dimensionless toughness $\mathcal{K}_m$, the ratio σ_o/σ_T and the dimensionless time defined as

$$\tau = t/t_{om}, \quad t_{om} = \frac{E'^2\mu'}{\sigma_o^3} \tag{15}$$

5. NUMERICAL ALGORITHM

We adopt a fixed regular grid and discretize elasticity by using displacement discontinuity method with piece-wise constant elements. The fluid mass conservation is discretized by finite difference. We use an implicit scheme to solve the fluid pressure and the associated opening. Our scheme consists of the use of two successive algorithms. In the beginning, denoted as the lag-initiation algorithm, we adopt an Elrod-Adams based method in order to automatically account for the appearance of the fluid lag. In a second stage, we use the results of the previous algorithm to initialize a simulation tracking the fluid front position via the introduction of a filling fraction variable as in Gordeliy and Detournay, 2011. This allows us to to perform simulations with a larger span of dimensionless time at a reduced computational cost. We choose the same element size in both algorithms, and solve iteratively for the time-step increment corresponding to a given increment of fracture length. A fully implicit time stepping method is used in both cases.

5.1. Lag-initiation algorithm

Overview We initiate the fracture aperture from the solution of a static elastic fracture under a uniform fluid pressure slightly larger than σ_o. For a given fracture length increment, the solution is obtained using three nested iterative loops: starting from a trial time step, we solve the fluid pressure for all elements inside the fracture using a quasi-Newton method. Such a procedure is repeated until all elements reach a consistent state: either fluid or vapor. A new estimate of the cohesive forces is obtained in another loop. We obtain the converged solutions on cohesive forces using fixed-point iterations with under-relaxation. The time step is adjusted iteratively in an outer loop using a bi-section and secant method in order to fulfill the propagation criterion.

Elasticity

$$\mathbb{A}\mathbf{w} = \mathbf{p}_f - \sigma_{coh}(\mathbf{w}) - \sigma_o \tag{16}$$

where $\mathbb{A}$ is the elastic matrix obtained via the discretization of the elastic operator using the displacement discontinuity method, $\mathbf{p}_f$, σ_o, σ_{coh} are the vectors of fluid pressure, confining stress and cohesive forces respectively.

Elrod-Adams lubrication A state variable θ is introduced in the mass conservation, characterizing the percentage of liquid occupying the fracture within a certain element as in Mollaali and Shen, 2018. All the elements inside the fracture can be classified into three domains.

$$\begin{aligned}
\eta_p &= \{i \in \eta_\Gamma \mid \theta_i = 1, \quad p_{fi} > 0\} \\
\eta_\theta &= \{i \in \eta_\Gamma \mid 0 < \theta_i < 1, \quad p_{fi} = 0\} \\
\eta_{ex} &= \{i \in \eta_\Gamma \mid i \notin (\eta_p \cup \eta_\theta), \quad p_{fi} = 0, \quad \theta_i = 0\}
\end{aligned} \tag{17}$$

where $\eta_p \cap \eta_\theta = \emptyset$, $\eta_\Gamma = \eta_p \cup \eta_\theta \cup \eta_{ex}$. For η_p, liquid is completely filled inside the element, while η_θ, η_{ex} corresponds to the fluid lag. The percentage of the liquid mass inside the fluid lag differs from $\eta_\theta (0 < \theta < 1)$ and $\eta_{ex} (\theta = 0)$. The lubrication equation integrated over element i writes as

$$\underbrace{\int_i \frac{\partial(\theta w)}{\partial t} \mathrm{d}x}_{1} + \underbrace{\int_i \frac{\partial}{\partial x}\left(-\frac{w^3}{\mu'}\frac{\partial p_f}{\partial x}\right)\mathrm{d}x}_{2} - \underbrace{\frac{Q_o}{2}\delta_{(i,1)}}_{3} = 0 \tag{18}$$

The first term is discretized as ,

$$\int_i \frac{\partial \theta w}{\partial t}\mathrm{d}x = \frac{1}{\Delta t} h(\theta_i w_i - \theta_i^o w_i^o) \tag{19}$$

where the superscript o denotes the solution at the previous time step. The second term is discretized as

$$\begin{aligned}
&\int_i \frac{\partial}{\partial x}\left(-\frac{w^3}{\mu'}\frac{\partial p_f}{\partial x}\right)\mathrm{d}x = \left[-\frac{w^3}{\mu'}\frac{\partial p_f}{\partial x}\right]_{i-1/2}^{i+1/2} \\
&= \frac{1}{\mu'} w_{i-1/2}^3 \left(\frac{p_{f,i} - p_{f,i-1}}{h}\right) - \frac{1}{\mu'} w_{i+1/2}^3 \left(\frac{p_{f,i+1} - p_{f,i}}{h}\right)
\end{aligned} \tag{20}$$

$$w_{i-1/2} = \frac{w_i + w_{i-1}}{2}, \quad w_{i+1/2} = \frac{w_i + w_{i+1}}{2} \tag{21}$$

where h is the element size.

After back-substituting the elasticity into the lubrication equation, we solve for $p_{f,i} (i \in \eta_p)$ and $\theta_i (i \in \eta_\theta)$ through a quasi-Newton method using the solution of the previous time step as an initial guess. The lag-initiation algorithm consists of updating the sets of η_p and η_θ as demonstrated in Table 2 , which is already implemented in Mollaali and Shen, 2018 to study the propagation of a linear elastic hydraulic fracture.

Propagation condition In the context of a cohesive zone, we check the equality of the tensile stress component ahead of the fracture tip with the material tensile strength:

$$\sigma_{yy,n+1} = A_{n+1,j} w_j - \sigma_o = \sigma_T, \quad j = 1 \ldots n \tag{22}$$

where n is the element number inside the fracture at the current time step.

In a linear elastic medium, the propagation condition is obtained by integrating the tip asymptote over the element closest to the fracture tip. The averaged opening for this element w_n is in function of K'

$$w_n = \frac{2}{3}\frac{K'\sqrt{h}}{E'} \tag{23}$$

Table 2: Algorithm using the Elrod-Adams model (adjusted from Mollaali and Shen, 2018) within one iteration with a given cohesive force vector

Repeat solving for $p_{f,i}$, θ_i for $i \in \eta_p \cup \eta_\theta$ using Newton's method;
for $i \in \eta_\Gamma$ **do**
  if $p_{f,i} < 0$ **then** set $p_{f,i} = 0$, $\eta_p \leftarrow \eta_p \setminus \{i\}$, $\eta_\theta \leftarrow \eta_\theta \cup \{i\}$, $\eta_{ex} \leftarrow \eta_\Gamma \setminus (\eta_p \cup \eta_\theta)$
  if $\theta_i > 1$ **then** set $\theta_i = 1$, $\eta_\theta \leftarrow \eta_\theta \setminus \{i\}$, $\eta_p \leftarrow \eta_p \cup \{i\}$, $\eta_{ex} \leftarrow \eta_\Gamma \setminus (\eta_p \cup \eta_\theta)$
  if $\theta_i < 0$ **then** set $\theta_i = 0$, $\eta_\theta \leftarrow \eta_\theta \setminus \{i\}$, $\eta_{ex} \leftarrow \eta_\Gamma \setminus (\eta_p \cup \eta_\theta)$
end
until $p_{f,i} \geq 0$, $0 \leq \theta_i \leq 1$ for $i \in \eta_\Gamma$ are satisfied.

5.2. Fluid-front-tracking algorithm

Overview The fluid-front tracking algorithm considers that there is a clear boundary between the injection fluid and cavity. By using a filling fraction ϕ, such code collects all the liquid mass in the fluid lag to one partially-filled element which is next to the fully-filled element (fluid channel element) nearest to the tip (denoted as the m^{th} element).

We solve the increment of the opening in the channel elements for a given fracture front through three nested loops. One tracks the fluid front, one updates the time step to fulfill the propagation condition and another solves the non-linear system due to the cohesive forces and lubricated fluid flow through a fixed-point scheme.

Elasticity

$$\mathbf{p}_c - \sigma_o - \sigma_{cohc} = \mathbb{A}_{cw}\mathbf{w} + \mathbb{A}_{ol}(-\sigma_o - \sigma_{cohl}) \tag{24}$$

where $\mathbf{p}_c$ is the vector net pressures in the channel part of the fracture; σ_{cohc} and σ_{cohl} cohesive forces applied in the fluid channel and fluid lag.

$$\begin{aligned} \mathbb{A}_{cw} &= \mathbb{A}_{cc} - \mathbb{A}_{cl}\mathbb{A}_{ll}^{-1}\mathbb{A}_{lc} \\ \mathbb{A}_{ol} &= \mathbb{A}_{cl}\mathbb{A}_{ll}^{-1} \end{aligned} \tag{25}$$

$\mathbb{A}_{cc}, \mathbb{A}_{cl}, \mathbb{A}_{lc}, \mathbb{A}_{ll}$ are sub-matrix of the elastic matrix $\mathbb{A}$ associated with elements inside the fluid channel and lag.

Lubrication flow For fluid channel elements ($1 \leq i \leq m$),

$$\begin{aligned} \Delta w_i =& \frac{\Delta t}{\mu' h^2}\left(w_{i-1/2}^3 p_{c,i-1} + w_{i+1/2}^3 p_{c,i+1}\right) \\ &- \frac{\Delta t}{\mu' h^2}(w_{i-1/2}^3 + w_{i+1/2}^3)p_{c,i} + \delta_{(i,1)}\frac{Q_o \Delta t}{2h} \\ &- \delta_{(i,m)}F_m - H(i - m^o)\sum_{k=m^o+1}^{m}\delta_{(i,k)}F_k \end{aligned} \tag{26}$$

The second term on the second line represents the contribution due to a constant injection rate and the two terms on the thrid line are mass corrections due to the partially-filled element where the fluid front locates. $H(\cdot)$ is the Heaviside step function.

$$F_m = \begin{cases} \phi w_{m+1} - \phi^o w_{m+1}^o, & m = m^o \\ \phi w_{m+1} - \phi^o w_{m^o+1}^o - \sum_{i=m+1}^{m^o} w_i, & m < m^o \end{cases} \tag{27}$$

$$F_k = \begin{cases} (1-\phi^o)w_k^o, & k = m^o + 1 \\ w_k^o, & k > m^o + 1 \end{cases} \tag{28}$$

where the superscript o refers to the solutions at the previous time step. The lubrication equation can be thus arranged as

$$\Delta\mathbf{w} = \mathbb{L} \cdot \mathbf{p}_c + \mathbf{S}_1 - \mathbf{S}_m - \mathbf{S}_{m^o} \tag{29}$$

Coupled system of equations We back-substitute the elasticity and write the coupled system as in Eq. (30). For a given fracture front and a trial time step, we solve for incremental apertures $\Delta\mathbf{w}$ using fixed-point iterations. The tangent linear system reads:

$$\begin{aligned} (\mathbb{I} - \mathbb{L}(\Delta\mathbf{w}^{(s-1)})\mathbb{A}_{cw})\Delta\mathbf{w}^s =& \mathbb{L}(\Delta\mathbf{w}^{(s-1)})\mathbb{A}_{cw}\mathbf{w}^o \\ &+ \mathbb{L}(\Delta\mathbf{w}^{(s-1)})\mathbb{A}_{ol}(-\sigma_o - \sigma_{cohl}(\Delta\mathbf{w}^{(s-1)})) \end{aligned} \tag{30}$$

where s refers to the formulation related to the solution of the previous iteration.

Update of the fluid front position The fluid front estimation is conducted based on the solution at the previous iteration.

$$\begin{aligned} \ell_f^{(s)} &= (m^o + \phi^o)h + V^{(s-1)}\Delta t, \\ m^{(s)} &= \text{floor}[\ell_f^{(s)}/h], \\ \phi^{(s)} &= \ell_f^{(s)}/h - m^{(s)} \end{aligned} \tag{31}$$

where V is the fluid front velocity and can be obtained through the fracture opening and net pressure,

$$\begin{aligned} V &= \frac{1}{2}\left(V^o - \frac{1}{\mu'}w_m^2\frac{\partial p}{\partial x}\right), \\ \frac{\partial p}{\partial x} &= \left(p_{c,m} - \frac{p_{c,m} + \sigma_o}{\phi + 1/2} - p_{c,m-1}\right)/(2h), \quad m > 1 \end{aligned} \tag{32}$$

The iteration starts with $V^{(0)} = V^o$ and continues until $|(\ell_f^{(s)} - \ell_f^{(s-1)})/\ell_f^{(s-1)}|$ is within a set tolerance.

5.3. Connection of the two algorithms

The fluid-front-tracking algorithm calls for the solution at the previous time step $(w^o, p_f^o, V^o, m^o, \phi^o, \ell_f^o)$ as an initial condition. Such a solution comes from the results of the lag-initiation / Elrod-Adams based algorithm at a chosen time step k. V^o is approximated by the velocity of the fluid front by using fluid front at the previous $(k-1)$ and the latter $(k+1)$ time step of the chosen one.

$$V^o = (\ell_{f,k+1} - \ell_{f,k-1})/(t_{k+1} - t_{k-1}) \tag{33}$$

where t_{k-1} and t_{k+1} are respectively propagation time at the $(k-1)^{\text{th}}$ and $(k+1)^{\text{th}}$ time step.

$m^o = m_o^k$ is the number of elements in the domain η_p at the time step k. ϕ^o is obtained by considering the fluid mass in the lag elements all gathered in the partially-filled element (the $(m_o^k + 1)^{\text{th}}$ element).

$$\phi^o = \sum_i \theta_i^k w_i^k / w_{m_o^k+1}, \quad i \in \eta_\theta \tag{34}$$

We get the initial guess of the fluid front through Eq. (31).

6. RESULTS AND DISCUSSIONS

6.1. Benchmark for LEFM

Several simulations using a linear elastic fracture mechanics criterion (no cohesive zone) have been carried out using different $\mathcal{K}_m$ values in order to benchmark our scheme. We present here the evolution of fluid fraction and dimensionless fracture length with dimensionless time spanning from $\tau = 10^{-9}$ to 1 as illustrated in Fig. 2 and Fig. 3. The solutions obtained from our calculation (CZMLAG) match well the numerical solutions reported in Lecampion and Detournay, 2007.

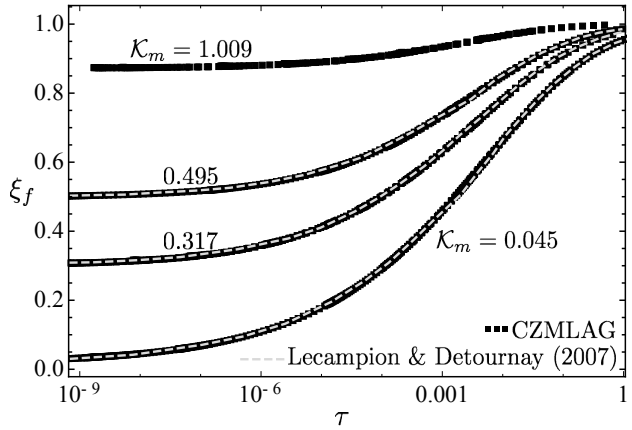

Fig. 2: Evolution of fluid front ξ_f for different $\mathcal{K}_m$

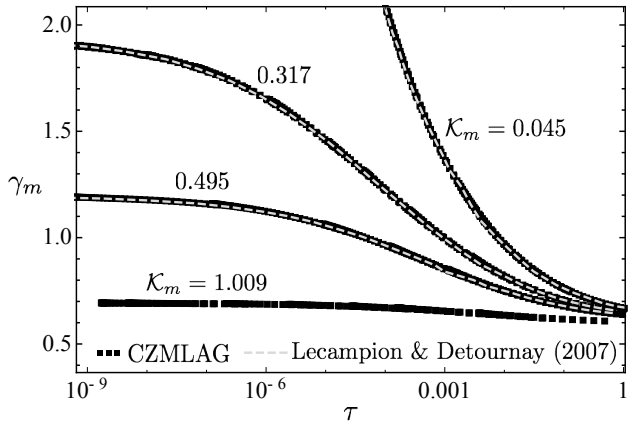

Fig. 3: Evolution of fracture length γ_m in viscosity scaling for different toughness $\mathcal{K}_m$

6.2. A stress-dependent numerical accuracy

The mesh size has a significant effect on the stress accuracy ahead of the tip and influences a lot the validity of the propagation criterion. By studying the stress field of a static fracture with uniform net pressure, we show that large σ_o/σ_T calls for more elements inside the cohesive zone to maintain the same stress accuracy, as shown in Fig. 4.

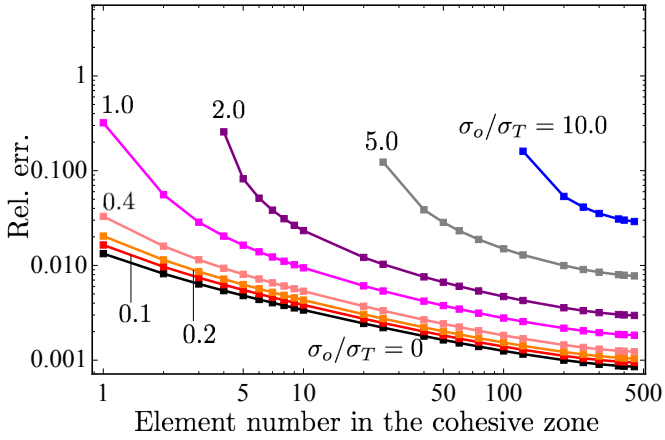

Fig. 4: Mesh dependency of the stress accuracy ahead of the fracture tip $\sigma_{yy,n+1}$ (stress component of the element nearest to the fracture tip). The relative error is calculated only when $\sigma_{yy,n+1}$ is in traction.

6.3. Effect of the solid non-linearity

We present in this section the numerical results of a permeable cohesive zone with $\mathcal{K}_m = 1.009$ and discuss briefly the impact of the solid non-linearity and the dimensionless ratio σ_o/σ_T on the fracture propagation. For all simulations shown here, there are sufficient elements in the cohesive zone to assure that the stress field calculation ahead of the fracture tip is around a tolerance of 1%.

In quasi-brittle materials, the cohesive zone develops and saturates after a certain time. We are more interested in the states with already a saturation of the cohesive zone. As il-

lustrated in Fig. 5, the length of the non-cohesive part of the fracture develops with time and slowly converge to the linear elastic curve. σ_o/σ_T determines the dimensionless time at which the non-cohesive fracture length begins to develop.

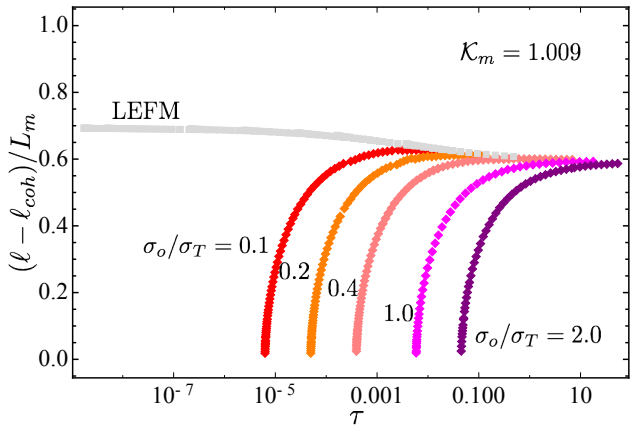

Fig. 5: Time evolution of the non-cohesive part of the fracture for different ratio σ_o/σ_T - - $\mathcal{K}_m = 1.009$ case.

The dimensionless fracture length presents an evolution similar to that of a linear elastic fracture, as shown in Fig. 6. However, the fluid fraction can be much less than the linear elastic case depending on the evaluated dimensionless time, as shown in Fig. 7.

As the propagation goes on, the fluid lag and cohesive zone take up less and less fraction of the whole fracture. For a given dimensionless toughness $\mathcal{K}_m$, a larger σ_o/σ_T makes it easier to keep the fluid front embedded inside the cohesive zone as shown in Fig. 8. The fluid lag can be much larger compared with an elastic fracture, as shown in Fig. 9.

Cohesive forces strengthen the suction effect associated with the fluid lag and confining stress. With a small amount of fluid pushed toward the fracture center, we observe an increase of the net pressure and fracture opening at the inlet as demonstrated in Fig. 10 and Fig. 11. The drop of the

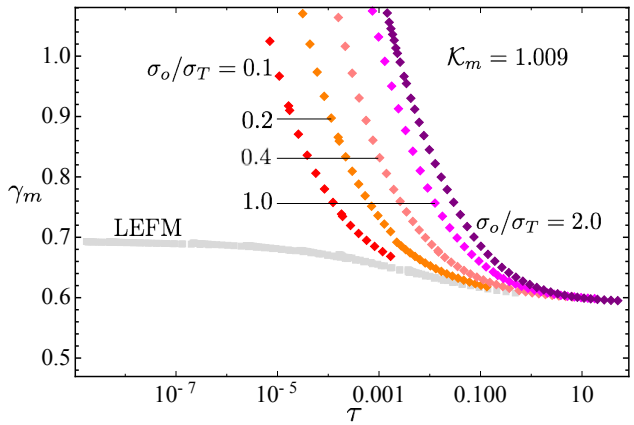

Fig. 6: Time evolution of the dimensionless fracture length $\gamma_m = \ell/L_m$ in viscosity scaling for different ratio σ_o/σ_T - - $\mathcal{K}_m = 1.009$ case.

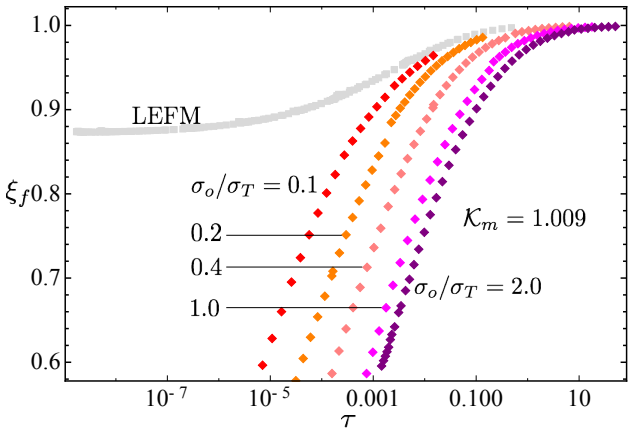

Fig. 7: Time evolution of the fluid fraction ξ_f for different ratio σ_o/σ_T - - $\mathcal{K}_m = 1.009$ case.

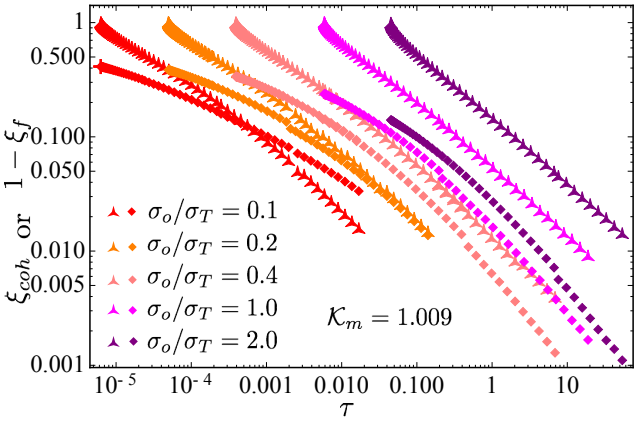

Fig. 8: Time evolution of cohesive length ξ_{coh} (shown as stars) and fluid lag $1 - \xi_f$ (shown as squares) in viscosity scaling for different ratio σ_o/σ_T - - $\mathcal{K}_m = 1.009$ case.

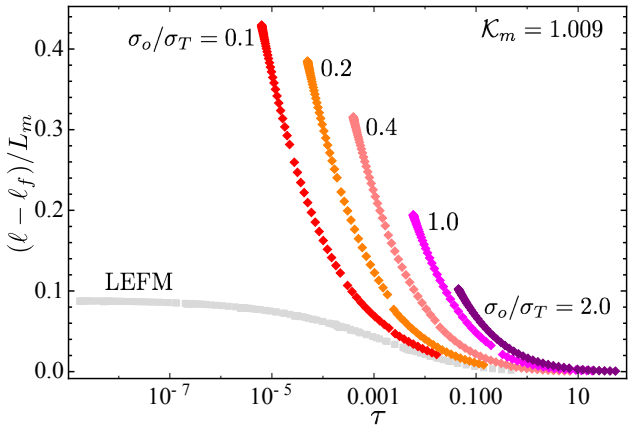

Fig. 9: Time evolution of fluid lag $(\ell - \ell_f)/L_m$ for different ratio σ_o/σ_T - - $\mathcal{K}_m = 1.009$ case.

pressure is localized near the tip because of the strengthened suction effect via cohesive traction, leading to a more uniform pressure distribution near the fracture center as shown in Fig. 12.

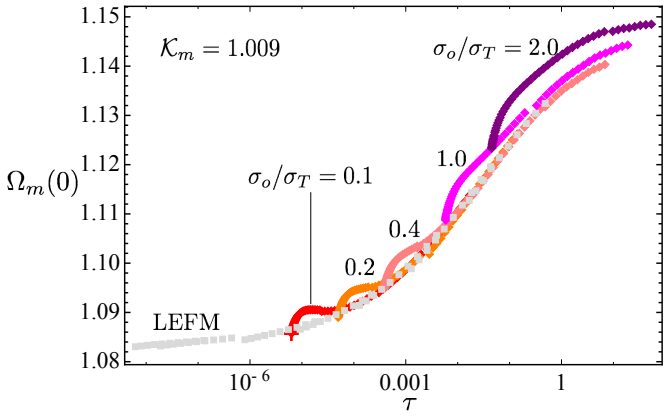

Fig. 10: Time evolution of the dimensionless opening at the fracture inlet - - $\mathcal{K}_m = 1.009$ case.

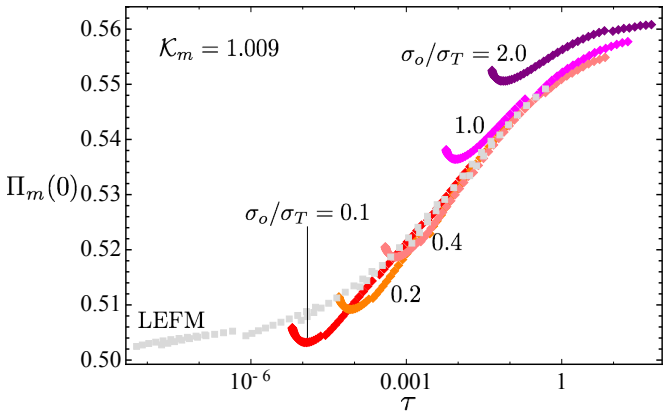

Fig. 11: Time evolution of the dimensionless net pressure at the inlet - - $\mathcal{K}_m = 1.009$ case.

7. CONCLUSION

We have studied the effect of solid non-linearity on the propagation of a plane-strain hydraulic fracture by considering the existence of a cohesive zone and a fluid lag. The suction associated with the fluid lag and the cohesive zone clamps the fracture tip, and further localizes the pressure drop. As a result, the opening and the net pressure increases when the cohesive zone becomes relatively small compared with the whole fracture. The propagation is not solely determined by the dimensionless toughness $\mathcal{K}_m$ (related to the fracture energy) and the time scale t_{om} but also by the ratio σ_o/σ_T. For a given $\mathcal{K}_m$ value, σ_o/σ_T determines the development of the cohesive zone and the evolution of the fluid lag.

The algorithm presented in this paper is very specific to the problem of a plane strain hydraulic fracture. However, it

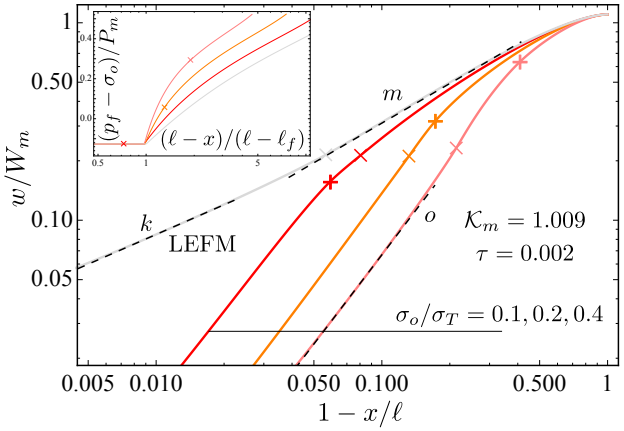

Fig. 12: Dimensionless opening and net pressure profiles at $\tau = 0.002$ for $\mathcal{K}_m = 1.009$ case. "+" indicates the boundary of the cohesive zone and "×" indicates the fluid front location.

can be easily extended to solve the equivalent axisymmetric fracture case. In spite of the simple geometry, it is already an extremely challenging effort for such algorithm dealing with several orders of magnitude of time and fracture extension. The numerical difficulty is mainly brought by the requirement of a sufficiently fine mesh to capture the small tensile zone ahead of the tip which is significantly shrinking for larger ratio σ_o/σ_T. Without the knowledge of an initial solution in the quasi-brittle case, the algorithm proposed here shows less computational cost compared with the lag-initiation algorithm. More work is still required in order to investigate larger ratio σ_o/σ_T as well as longer fracture propagation.

REFERENCES

1. Bunger, A.P., 2005. *Near-surface hydraulic fracture*, Ph.D. thesis, University of Minnesota.

2. Carrier, B. and Granet, S., 2012. Numerical modeling of hydraulic fracture problem in permeable medium using cohesive zone model, *Eng. Fract. Mech.*, 79, 312–328.

3. Chen, Z., 2012. Finite element modelling of viscosity-dominated hydraulic fractures, *J. Pet. Sci. Eng.*, 88, 136–144.

4. Chen, Z., Bunger, A., Zhang, X., and Jeffrey, R.G., 2009. Cohesive zone finite element-based modeling of hydraulic fractures, *Acta Mech. Solida Sin.*, 22 (5), 443–452.

5. Garagash, D.I., 2006. Propagation of a plane-strain hydraulic fracture with a fluid lag: Early-time solution, *Int. J. Solids and Struct*, 43 (18–19), 5811 – 5835.

6. Garagash, D.I., 2015. How fracking can be tough, IMA Workshop Hydraulic Fracturing Modeling and Simulation to Reconstruction and Characterization, University of Minnesota.

7. Garagash, D.I. and Detournay, E., 2000. The tip region of a fluid-driven fracture in an elastic medium, *J. Appl. Mech.*, 67, 183–192.

8. Gordeliy, E. and Detournay, E., 2011. A fixed grid algorithm for simulating the propagation of a shallow hydraulic fracture with a fluid lag, *Int. J. Numer. Anal. Methods Geomech.*, 35 (5), 602–629.

9. Hills, D.A., Kelly, P., Dai, D., and Korsunsky, A., 2013. *Solution of crack problems: the distributed dislocation technique*, vol. 44, Springer Science & Business Media.

10. Lecampion, B., 2012. Hydraulic fracture initiation from an open-hole: Wellbore size, pressurization rate and fluid-solid coupling effects, *in: 46th U.S. Rock Mechanics/Geomechanics Symposium*, Chicago, Illinois.

11. Lecampion, B. and Detournay, E., 2007. An implicit algorithm for the propagation of a hydraulic fracture with a fluid lag, *Comput. Methods Appl. Mech. Eng.*, 196 (49-52), 4863–4880.

12. Li, Y., Deng, J., Liu, W., and Feng, Y., 2017. Modeling hydraulic fracture propagation using cohesive zone model equipped with frictional contact capability, *Comput. Geotech.*, 91, 58–70.

13. Moës, N. and Belytschko, T., 2002. Extended finite element method for cohesive crack growth, *Eng. Fract. Mech.*, 69 (7), 813–833.

14. Mollaali, M. and Shen, Y., 2018. An Elrod–Adams-model-based method to account for the fluid lag in hydraulic fracturing in 2D and 3D, *Int. J. Fract.*, 211 (1-2), 183–202.

15. Papanastasiou, P., 1997. The influence of plasticity in hydraulic fracturing, *Int. J. Fract.*, 84 (1), 61–79.

16. Rubin, A.M., 1993. Tensile fracture of rock at high confining pressure: implications for dike propagation, *J. Geophys. Res. Solid Earth*, 98 (B9), 15919–15935.

17. Salimzadeh, S. and Khalili, N., 2015. A three-phase XFEM model for hydraulic fracturing with cohesive crack propagation, *Comput. Geotech.*, 69, 82–92.

18. Sarris, E. and Papanastasiou, P., 2011. Modeling of hydraulic fracturing in a poroelastic cohesive formation, *Int. J. Geomech.*, 12 (2), 160–167.

19. Shen, Y., 2014. A variational inequality formulation to incorporate the fluid lag in fluid-driven fracture propagation, *Comput. Methods Appl. Mech. Eng.*, 272, 17–33.

20. Shlyapobersky, J., 1985. Energy analysis of hydraulic fracturing, *in: The 26th US Symposium on Rock Mechanics (USRMS)*, Rapid City, South Dakota.

21. Shlyapobersky, J., Wong, G., and Walhaug, W., 1988. Overpressure calibrated design of hydraulic fracture stimulations, *in: SPE Annual Technical Conference and Exhibition*, Houston, Texas, 133–148.

22. Thallak, S., Holder, J., and Gray, K., 1993. The pressure dependence of apparent hydrofracture toughness, *in: The 34th US Symposium on Rock Mechanics (USRMS)*, Madison, Wisconsin.

23. Wang, H., 2015. Numerical modeling of non-planar hydraulic fracture propagation in brittle and ductile rocks using XFEM with cohesive zone method, *J. Pet. Sci. Eng.*, 135, 127–140.

24. Wang, H., Marongiu-Porcu, M., and Economides, M.J., 2016. Poroelastic and poroplastic modeling of hydraulic fracturing in brittle and ductile formations, *SPE Prod. Oper.*, 31 (01), 47–59.

25. Yao, Y., Liu, L., and Keer, L.M., 2015. Pore pressure cohesive zone modeling of hydraulic fracture in quasi-brittle rocks, *Mech. Mater.*, 83, 17–29.

26. Zhang, X., Jeffrey, R., and Detournay, E., 2005. Propagation of a hydraulic fracture parallel to a free surface, *Int. J. Numer. Anal. Methods Geomech.*, 29 (13), 1317–1340.